ELSEVIER

Thermochimica Acta 323 (1998) 123–130

thermochimica acta

Precipitation kinetics in solutionized aluminum alloy 2124: II. Effect of prior Guinier–Preston zone formation

George W. Smith*

Physics and Physical Chemistry Department, General Motors Research and Development Center, Warren, MI 48090-9055, USA

Received 19 February 1998; received in revised form 14 July 1998; accepted 27 July 1998

Abstract

Part I of this study described a calorimetric investigation of kinetics and energetics of Guinier–Preston (GP) zone formation and precipitation in solutionized (SOL) aluminum alloy 2124. The present paper discusses results of experiments designed to determine the effect of prior GP zone formation on precipitation in the same alloy. The samples studied (designated SOL/GP samples) had each been held at temperatures $\leq 100^{\circ}C$ until GP zone formation was determined to be complete, after which differential scanning calorimetry (DSC) and differential isothermal calorimetry (DIC) precipitation measurements were carried out. The DSC data (for scan rates from 1.2 to 20°C/min) were analyzed by the Kissinger method to yield activation energies and time constants. From the DIC experiments, we obtained precipitation kinetics information using analysis techniques developed in this laboratory. Precipitation activation energies and time constants for SOL/GP samples derived from DSC agree rather well with those from DIC. As was the case for the SOL alloy, two processes with slightly different temperature ranges are involved in precipitation in SOL/GP 2124. Although prior GP zone formation seems to have little effect on the first precipitation process (associated with S' ($CuMgAl_2$)), it does reduce the activation energy of the second one (assigned to θ' ($CuMg_2$)) by more than 10%. The exothermic heat of precipitation, ΔQ (measured isothermally) is also relatively unaffected by previous GP zone formation.

Keywords: Differential isothermal calorimetry; Differential scanning calorimetry; Guinier–Preston zones; Precipitation kinetics; Solutionized aluminum alloy 2124

1. Introduction

This paper continues prior calorimetric studies [1,2] intended to enhance our understanding of precipitation in aluminum alloys. In Part I [1] of this study, activation energies and time constants for Guinier–Preston (GP) zone formation and precipitation in solutionized (SOL) alloy 2124 were determined by both differential scanning calorimetry (DSC) and differential isothermal calorimetry (DIC). The two methods agreed rather well. The present paper extends that work to investigate the effect of prior GP zone formation on precipitation in alloy 2124.

2. Experimental aspects, results and analyses

The experimental methods and analytical techniques have been described previously [1–4], so only a brief review is presented here.

*Corresponding author. Tel.: +1-810-986-0614; fax: +1-810-986-3091; e-mail: George_W._Smith@notes.gmr.com

0040-6031/98/$ – see front matter
PII: S0040-6031(98)00513-9

2.1. Samples

The composition, preparation and solution treatment of the 2124 aluminum alloy were discussed in Part I. In that work, the kinetics of GP zone formation in some SOL samples were determined isothermally at temperatures, T_{GP} ($\leq$100°C). During those studies, GP zone formation was allowed to proceed to completion (as determined by monitoring heat evolution). The samples were then removed from the calorimeter and immediately placed in a cold chamber at −74°C, where they remained until just prior to the present DSC and DIC studies. These samples are hereafter referred to as SOL/GP to indicate that they had been 'aged' isothermally in the temperature range for GP zone formation. In each case, T_{GP} was sufficiently low so that GP zone dissolution should not have occurred.

2.2. Calorimetry

The kinetics and energetics of precipitation were determined using Perkin–Elmer DSC2 and DSC7 differential scanning calorimeters. The DSC7 was operated in its temperature-scanning mode and the DSC2 in its isothermal mode. In the scanning mode the DSC instrument records the temperature dependence of dQ/dt, the rate of heat absorption or emission by the sample, at various temperature scan rates. Endothermic or exothermic events appear as peaks superimposed on the baseline. In a typical isothermal experiment, the temperature is increased rapidly (320°C/min) from −73°C to the experimental temperature T, at which the calorimeter records dQ/dt vs. t. As for DSC scans, dQ/dt curves in a DIC experiment can be either endothermic or exothermic. The total energy, ΔQ, absorbed or released during the isothermal process is determined by integrating dQ/dt vs. t.

2.3. DSC results and analysis

2.3.1. DSC scans

Fig. 1 shows DSC scans from [1] for samples of solutionized alloy 2124 at several temperature scan rates, S. Because of factors involving the calorimeter's equilibration time [1], we restricted S to $\leq$20°C/min. The scans of the SOL samples in Fig. 1 should be compared to those for SOL/GP samples in Fig. 2. It is apparent that the only feature lacking in the SOL/GP scans is the prominent GP zone formation peak seen in

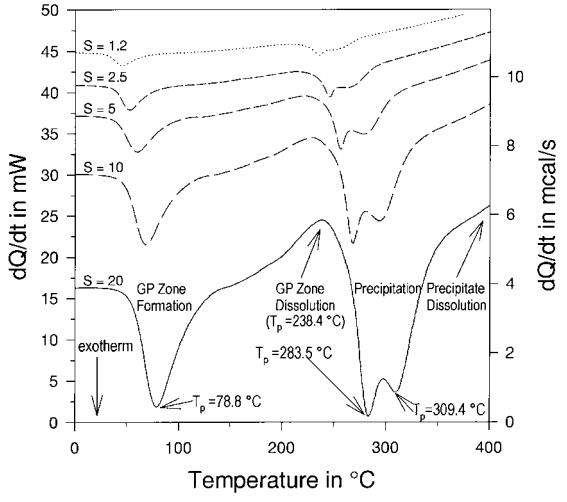

Fig. 1. dQ/dt vs. temperature for SOL alloy 2124 at scan rates, S, ranging from 1.2 to 20°C/min. Clearly visible are a GP zone formation exotherm (below 100°C), two precipitation exotherms (near 300°C), and two dissolution endotherms: GP zones (above 200°C) and precipitates (above 350°C). These DSC scans should be compared to those in Fig. 2. The curves are shifted vertically to avoid overlap.

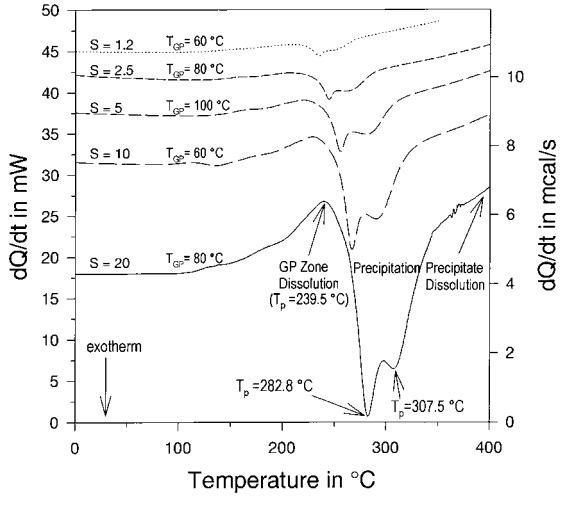

Fig. 2. Plots of dQ/dt vs. temperature for SOL/GP alloy 2124 at scan rates, S, from 1.2 to 20°C/min. T_{GP}, the temperature of the prior isothermal GP formation experiment, is indicated on each scan. Although the scans each lack a GP zone formation exothermic peak, in other respects they are nearly identical to those of Fig. 1.

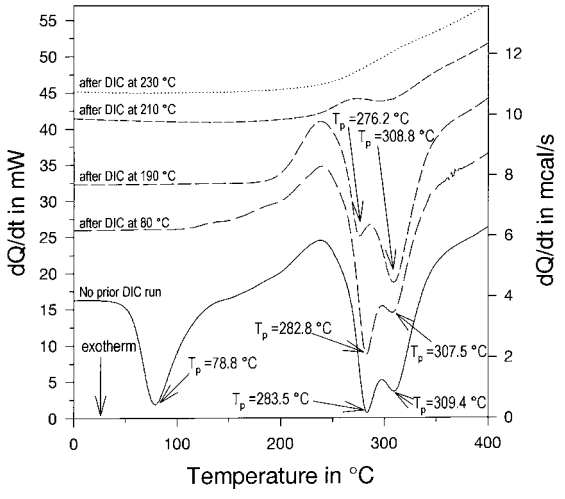

Fig. 3. Plots of dQ/dt vs. temperature at 20°C/min for samples of solutionized alloy 2124 which show the effect of prior DIC experiments on the precipitation peaks. It appears that GP zone dissolution is not greatly affected by prior treatment at temperatures as high as 190°C.

the SOL scans of Fig. 1. Above 150°C, in the GP zone dissolution and precipitation temperature ranges, the SOL/GP scans appear to be almost identical to those of the SOL samples.

The SOL/GP samples had been aged at T_{GP} values ranging from 60° to 100°C. The exact choice of T_{GP} did not seem to affect the observed DSC curve so long as GP zone dissolution did not occur. Dissolution did not, in fact, take place during either aging (the maximum T_{GP} value (100°C) was sufficiently low) or storage at −74°C. This conclusion is supported by Fig. 3 which shows the effect of heat treatment on subsequent DSC scans. Even after prior treatment at temperatures as high as 190°C, a GP zone dissolution endotherm is prominent at a temperature near 250°C. However, the first precipitation peak is weakened and shifted to higher T (presumably due to a certain amount of precipitation), while the second peak remains almost unaffected. Prior treatment at temperatures >200°C removes most evidence of both precipitation peaks in subsequent DSC scans.

2.3.2. Kissinger analysis

Activation energies and rate constants are derived from the scan-rate dependence of T_p by means of an analysis pioneered by Kissinger [5–10]. Since the method has been discussed elsewhere and shown to be valid for overlapping peaks [1,2], it suffices to list the basic equations at this time:

$$\ln(T_p^2/S) = E_{act}/(RT_p) + \ln(E_{act}/Rk_0). \quad (1)$$

$$k = k_0 \exp(-E_{act}/RT) \ [\text{or } \tau \equiv 1/k = \tau_0 \exp(E_{act}/RT)]. \quad (2)$$

$$k_p = (E_{act}/R) \times (S/T_p^2), \quad (3)$$

Here, E_{act} is the activation energy for the process associated with a given peak, R the gas constant, and k_0 the pre-exponential factor in the Arrhenius equation for the rate constant k. Eq. (3), obtained by substitution of Eq. (2) into Eq. (1), gives the value of k at temperature T_p. In Eqs. (1) and (3), the scan rate S must be expressed in units of K/s (or °C/s) so that k will have the unit s^{-1}. It has been shown that DSC/Kissinger time constants, $1/k$, agree rather well with time constants derived from DIC experiments [1,2].

Kissinger plots for the GP zone dissolution peak and the first and second precipitation peaks were derived from the scans of Fig. 2 for the SOL/GP samples. The plots appeared similar to those obtained for SOL samples [2]. In each case, Eq. (1) fits the data very well; the derived Kissinger parameters are given in Table 1. (The E_{act} values for SOL/GP 2124 will be compared to those for SOL 2124 in Table 3). The activation energies and associated time constants for the three processes will be discussed in greater detail in Section 3.

2.4. DIC results and analyses

2.4.1. Isothermal dQ/dt curves

Kinetics of GP zone dissolution cannot be determined by isothermal calorimetry [1]. However, DIC experiments yield details concerning precipitation which are unobtainable from DSC. In Figs. 4–6 DIC curves for precipitation in SOL/GP samples at three different temperatures are compared to the corresponding curves for SOL samples. Scrutiny of the isotherm pairs reveals differences, which, although small, may be significant. For example, the decay process at long times seems somewhat faster in the SOL/GP samples. In addition, at 220°C (closest of the three to the GP zone formation region), the curve for the SOL sample becomes exothermic earlier than that for the SOL/GP sample (Fig. 4). This small initial

Table 1
Parameters for Kissinger fits to scanning experiments SOL/GP alloy 2124

T_{GP} [a]/°C	S [b]/(°C/min)	T_p [c]/°C	$1000/T_p$	ln (T_p^2/S)	Fit of Eq. (1)
A. GP zone dissolution endotherm		From Eq. (2): k_0=7.17 (+42.3/−6.12)×10^{13} s^{-1}			
60	1.2	204.3	2.0941	16.25	16.13
80	2.5	210.3	2.0681	15.54	15.65
100	5	220.0	2.0275	14.89	14.91
60	10	228.6	1.9930	14.23	14.28
80	20	239.5	1.9506	13.58	13.51
B. 1st Precipitation exotherm		From Eq. (2): k_0=2.655 (+9.26/−1.92)×10^{10} s^{-1}			
60	1.2	234.9	1.9681	16.37	16.29
80	2.5	244.6	1.9314	15.68	15.71
100	5	255.7	1.8908	15.03	15.08
60	10	267.0	1.8511	14.38	14.46
80	20	282.8	1.7986	13.74	13.65
C. 2nd Precipitation exotherm		From Eq. (2): k_0=1.302 (+4.06/−0.98)×10^{7} s^{-1}			
60	1.2	244.0	1.9335	16.41	16.45
80	2.5	259.4	1.8775	15.73	15.77
100	5	280.1	1.8074	15.12	14.92
60	10	290.1	1.7754	14.46	14.53
80	20	307.5	1.7219	13.83	13.88

[a] Temperature of prior DIC GP zone formation experiment.
[b] Temperature scan rate.
[c] DSC peak temperature.

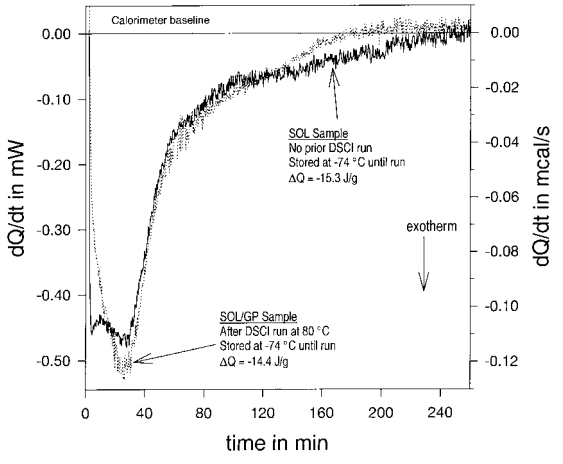

Fig. 4. Isothermal calorimetry curves of dQ/dt vs. time for precipitation in SOL and SOL/GP samples of alloy 2124 at 220°C.

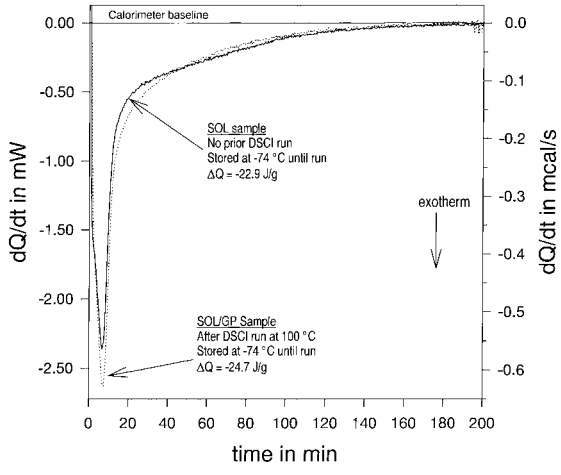

Fig. 5. Isothermal calorimetry curves of dQ/dt vs. time for precipitation in SOL and SOL/GP samples of alloy 2124 at 240°C.

exothermic contribution may be due to the rapid formation of GP zones after which they dissolve quickly to initiate precipitation. Since the differences between pairs of curves in Figs. 4–6 are small, the best way to assess effects of prior GP formation on precipitation is to compare time constants and activation energies for the SOL and SOL/GP alloys.

2.4.2. Time constants and activation energies

The delay time, t_{peak}, is the time at which dQ/dt reaches its peak value, obeying an Arrhenius-like Eq. (1):

$$\ln t_{peak} = \ln t_0 + E_{act}/RT \quad (4)$$

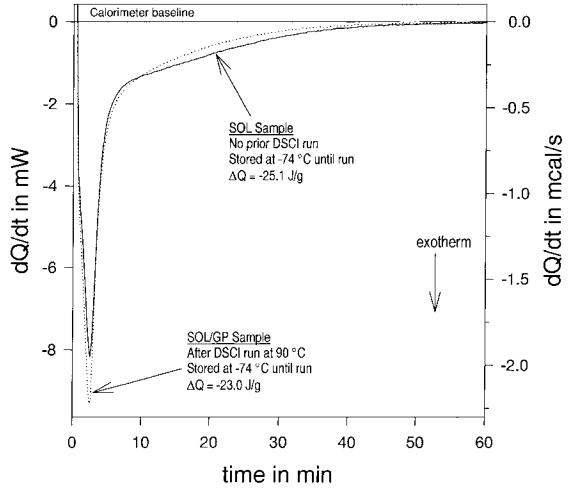

Fig. 6. Isothermal calorimetry curves of dQ/dt vs. time for precipitation in SOL and SOL/GP samples of alloy 2124 at 260°C.

Additional time constants are obtained from fits of analytical expressions to the decaying portion of dQ/dt [1,2,4]. One such analysis is a 2-exponential fit, from which two time constants (τ_1 and τ_2) are determined. Activation energies can be derived from Arrhenius plots of these time constants.

The 2-exponential analysis was originally developed [2] to take account of precipitation involving two species. In this case, the rate of heat evolution is given by

$$dQ/dt = -\alpha_1 \exp(-t/\tau_1) - \alpha_2 \exp(-t/\tau_2). \quad (5)$$

As shown in Part I, the fast and slow time constants (τ_1 and τ_2) of Eq. (5) should be compared to the Kissinger time constants ($1/k_1$ and $1/k_2$) for the first and second precipitation peaks.

Arrhenius plots of t_{peak} and the time constants, τ_1 and τ_2, for precipitation in SOL/GP alloy 2124 are similar in appearance to those for the SOL samples [2]. Values of t_{peak} and parameters for the 2-exponential analyses are given in Table 2. Activation energies for precipitation in SOL/GP 2124 are compared with those for the SOL alloy in Table 3.

As mentioned above, integration of DIC curves yields values of ΔQ, the heat released during precipitation. Fig. 7 presents a comparison between plots of ΔQ vs. temperature for SOL and SOL/GP 2124 samples. There is little difference between the two sets of data, suggesting that the effect of prior GP zone formation on subsequent precipitation is small.

Table 2
Peak and 2-exponential analyses of isothermal experiments precipitation in SOL/GP alloy 2124

			Peak [c]	2-exponential analysis [c]				
T_{GP} [a]/°C	T [b]/°C	$-\Delta Q$/(J g^{-1})	t_{peak}/(min)	α_1/(mW)	α_2/(mW)	τ_1/(min)	τ_2/(min)	r^2 [d]
80	210	13.14	15.00	0.100	0.193	96.93	97.24	0.93881
50	220	14.91	27.05	2.874	0.405	13.37	60.317	0.98378
80	220	14.42	25.57	4.901	0.445	10.82	60.19	0.98787
70	230	21.13	12.96	13.570	0.733	5.05	48.56	0.99731
75	230	16.92	12.68	9.442	0.399	5.949	57.59	0.98722
100	240	23.84	6.89	34.124	0.994	2.737	41.69	0.99728
70	240	24.32	6.47	42.791	1.394	2.309	27.58	0.99737
85	250	24.45	3.56	56.106	1.593	1.594	22.6	0.99774
60	260	24.75	2.36	99.064	3.921	1.004	9.792	0.99948
90	260	24.90	2.33	115.109	2.850	0.9601	12.72	0.99965
70	270	26.10	1.70	79.331	4.832	0.9535	7.168	0.99895
30, 70	280	25.01	0.90	37.453	3.371	1.538	5.115	0.99967
40, 70	300	22.97	0.48	86.043	14.797	0.5906	1.766	0.99994

[a] Temperature(s) of prior DIC GP zone formation experiment(s).
[b] Temperature of isothermal precipitation experiment.
[c] Parameters in columns 3–8 are defined in text and were determined at temperature T for each sample.
[d] r^2 is a measure of goodness of fit of DIC curves to Eq. (5).
The last two samples were the only ones subjected to two prior isothermal treatments in the GP zone formation temperature range.

Table 3
Activation energies (kJ/mol) for GP zone dissolution and precipitation in alloy 2124

Scanning/Kissinger analysis		E_{act}(SOL/GP)	E_{act}(SOL [a])
GP zone dissolution peak		152.4±8.0	159.9±5.4
1st Precipitation peak		129.4±6.3	131.1±5.9
2nd Precipitation peak		100.9±6.3	113.9±5.0
Isothermal analyses	E_{act} (t_{peak})	E_{act} (τ_1)	E_{act} (τ_2)
Precipitation (SOL/GP)	125.2±3.3	123.1±9.6	98.0±9.2
Precipitation (SOL [a])	118.9±6.3	127.7±15.1	111.3±8.8

[a] Results for SOL Alloy 2124 are from Ref. [1].

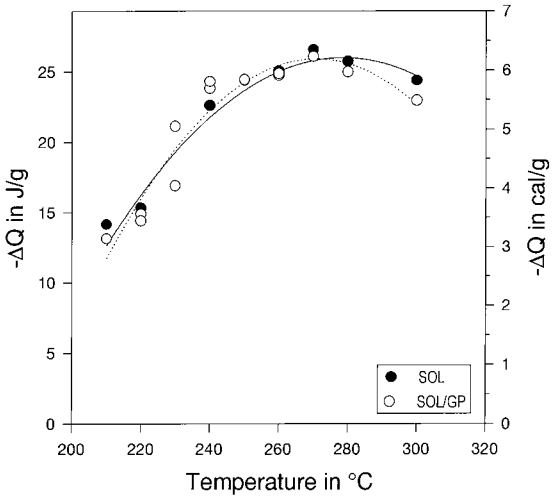

Fig. 7. Heat released, ΔQ, during precipitation in SOL and SOL/GP 2124 at various temperatures. ΔQ values were determined from isothermal calorimetry curves of dQ/dt vs. time. Curves are quadratic regression fits to data.

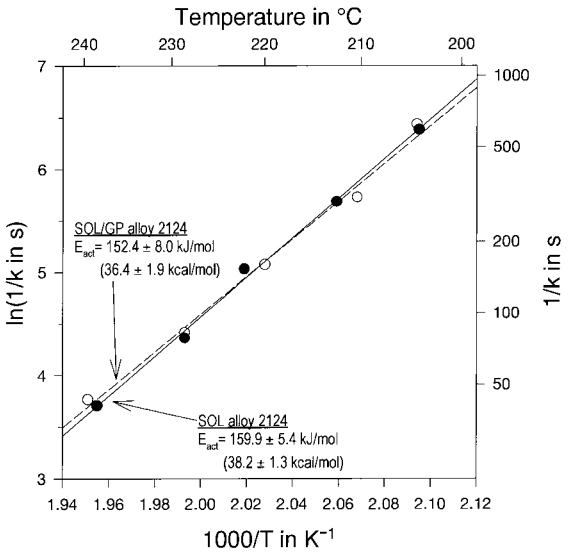

Fig. 8. Comparison of Arrhenius plots of 1/k derived from Kissinger analysis of GP zone dissolution peaks in SOL and SOL/GP 2124. Lines are best fits to the data. Closed symbols are for SOL samples, open symbols for SOL/GP.

3. Discussion: comparison of SOL and SOL/GP results

3.1. GP zone dissolution

The Kissinger activation energy for GP zone dissolution in SOL/GP 2124 is equal (within experimental error) to that for SOL 2124 (see Table 3). Furthermore, plots of the Kissinger time constant, 1/k, for the two systems are nearly identical (Fig. 8). Extrapolation of 1/k to lower temperatures shows that GP zone dissolution in alloy 2124 should take longer than 750 h at 100°C. This result supports our discussion of Fig. 3, where we argued that dissolution is slow at temperatures below ~190°C.

3.2. Precipitation

As pointed out in the foregoing and in Part I, precipitation in alloy 2124 involves both, fast and slow processes. Mishra's TEM studies [11] have indicated that the fast process is associated with the formation of S' ($CuMgAl_2$) and the slow one with θ' ($CuAl_2$). As seen in Table 3, Kissinger analyses of the two DSC precipitation peaks for SOL/GP samples yield activation energies (129 and 101 kJ/mol) which are essentially identical to those (123 and 98 kJ/mol) from 2-exponential fits of DIC curves. Both techniques agree that, for the fast precipitation process (1/k_1

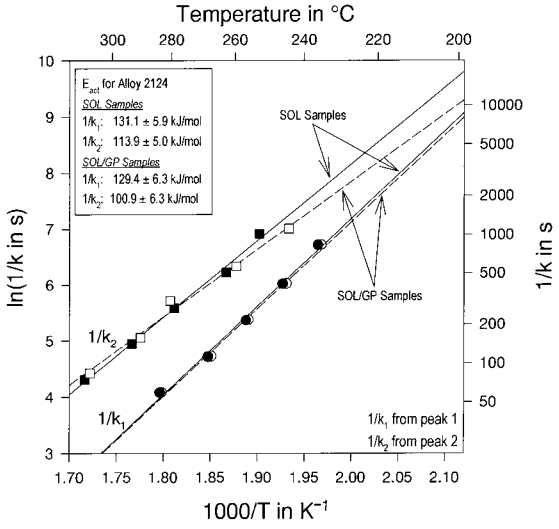

Fig. 9. Arrhenius plots of $1/k$ for fast (k_1) and slow (k_2) precipitation processes derived from Kissinger analyses of first and second DSC precipitation peaks for SOL and SOL/GP 2124. Lines are best fits to the data. Closed symbols are for SOL samples, open symbols for SOL/GP.

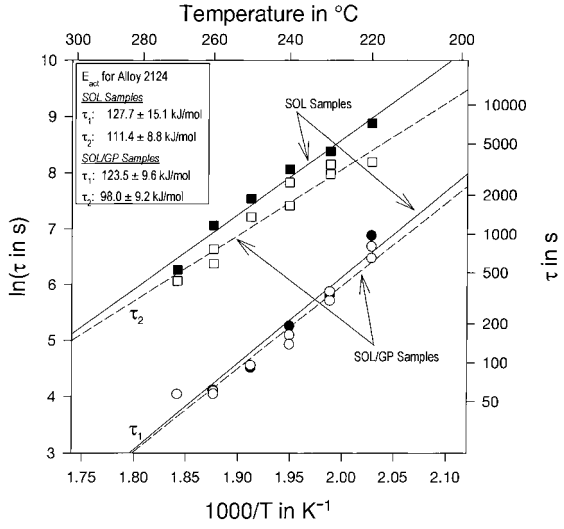

Fig. 10. Arrhenius plots of τ_1 and τ_2 from 2-exponential fit for precipitation in SOL and SOL/GP 2124. Lines are best regression fits to the data. Closed symbols are for SOL samples, open symbols for SOL/GP.

or τ_1) in SOL/GP samples, the activation energy is equal to that for SOL samples, but that for the slow process ($1/k_2$ or τ_2) E_{act} of SOL/GP 2124 is at least 10% lower than that for the SOL alloy. The activation energy derived from t_{peak} (125 kJ/mol) is comparable to that for the faster precipitation process ($1/k_1$ or τ_1) and is a few percent higher than that for the SOL samples (the difference being comparable to the experimental error).

Kissinger time constants ($1/k$) for both sets of samples are plotted in Fig. 9: although $1/k_1$ values for SOL/GP 2124 are essentially equal to those for SOL 2124, $1/k_2$ values for the SOL/GP samples deviate noticeably from those for the SOL samples to give the lower activation energy discussed in the previous paragraph. Similar behavior is seen for the DIC 2-exponential time constants (Fig. 10). As was the case for SOL samples [1], τ_1 and τ_2 differ from one another to a greater extent than do $1/k_1$ and $1/k_2$ (Fig. 11). The fact that prior GP zone formation affects E_{act} for the second precipitation process (but not that for the first) may indicate that the zones are chemically related to the second precipitate. A complete understanding of this curious result requires a more detailed TEM study.

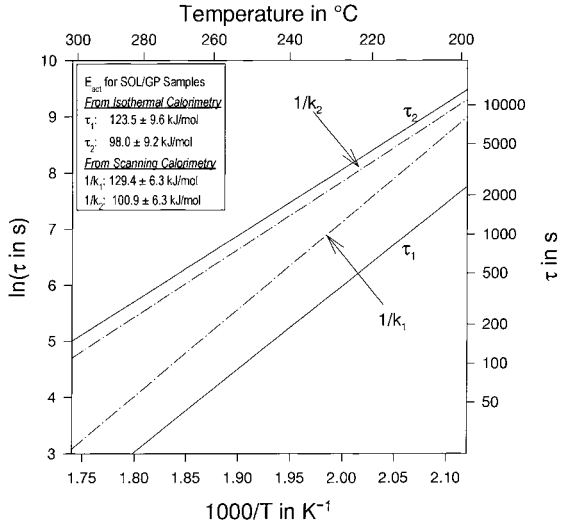

Fig. 11. Comparison of Arrhenius plots of regression fits to fast and slow time constants from DSC ($1/k_1$ and $1/k_2$) and DIC (τ_1 and τ_2) for SOL/GP 2124.

Acknowledgements

I thank Jody Hall and Anil Sachdev for the samples, Raja Mishra for sharing his TEM results, Spud Willett for heat treating the samples, Dick Hall for machining

them, Dan Hayden for computer programs, Dusanka Radovic for DSC scans, and Bill Baxter for useful comments.

References

[1] G.W. Smith, Thermochim. Acta 317 (1998) 7.
[2] G.W. Smith, Thermochim. Acta 313 (1998) 27.
[3] G.W. Smith, Scripta Met. et Mat. 31 (1994) 357.
[4] G.W. Smith, Thermochim. Acta 291 (1997) 59.
[5] H.E. Kissinger, Anal. Chem. 29 (1957) 1702.
[6] T. Ozawa, J. Thermal Anal. 2 (1970) 301.
[7] E.J. Mittemeijer, A. van Gent, P.J. van der Schaaf, Met. Trans. 17A (1986) 1441.
[8] E.J. Mittemeijer, L. Cheng, P.J. van der Schaaf, C.M. Brakman, B.M. Korevaar, Met. Trans. 19A (1988) 925.
[9] M. van Rooyan, E.J. Mittemeijer, Met. Trans. 20A (1989) 1207.
[10] H. Yinnon, D.R. Uhlmann, J. Non-Crystalline Solids 54 (1983) 253.
[11] R.K. Mishra, private communication, to be published.